中国激光

基于Nano-ICG增强巨噬细胞活体光声成像的急性呼吸道炎症无创定量评估

张建[1,2]，梁超豪[1]，罗志佳[1]，孟凡[1]，张艺晴[1]，王倩[1*]

[1]广州医科大学生物医学工程学院医学影像创新实验室，广东 广州 511436；
[2]广州医科大学附属第一医院呼吸疾病国家重点实验室，广东 广州 510120

摘要 巨噬细胞作为炎症阶段的主要吞噬细胞，其高表达是急性呼吸道炎症发展过程的临床特征之一。目前还没有一种成像方法能够以深组织穿透性和高分辨率的方式呈现巨噬细胞在急性炎症中的表达。以吲哚菁绿纳米颗粒（Nano-ICG）作为一种高效的光声成像（PAI）增强造影剂，评估了急性呼吸道炎症中巨噬细胞的表达量。激光共聚焦显微镜下的成像效果证实，Nano-ICG能够快速地被巨噬细胞吞噬。利用Nano-ICG增强光声成像效果后，气管内的PAI结果显示了巨噬细胞在炎症后气管壁上的分布区域。Nano-ICG增强的光声成像能够无创、定量地评估急性呼吸道炎症的发展程度，有望为呼吸疾病相关基础研究和临床诊疗提供新的影像技术支持。

关键词 医用光学；光声成像；急性呼吸道炎症；吲哚菁绿纳米颗粒；巨噬细胞

中图分类号 O439　　**文献标志码** A　　　　　　　　　　　　**DOI:** 10.3788/CJL231378

1 引　　言

呼吸道感染是全球负担最重的疾病之一，也是儿童死亡的主要原因之一[1-2]。仅统计5岁以下的儿童数据，世界各地每年因呼吸道病毒感染而死亡的人数高达300万人[3]。呼吸道病毒具有感染力强、传播快、潜伏期短、发病急等特点，在世界范围内广泛流行，已经严重影响全球儿童健康，造成了巨大的经济损失和人员伤亡。

细菌感染是引起急性呼吸道炎症的主要因素。其中，革兰氏阴性菌的感染与急性呼吸窘迫综合征（ARDS）、慢性阻塞性肺病（COPD）急性加重[4]以及哮喘急性发作[5]中的气道炎性损伤密切相关。革兰阴性细菌细胞壁外膜上的脂多糖（LPS）成分又称为内毒素，是革兰氏阴性杆菌致病的抗原，目前被广泛用于构建急性呼吸道炎症模型[6-8]。典型的急性炎症具有四个基本体征：发红、局部发热、肿胀和疼痛。在较小的范围内，炎症表现为对局部损伤或感染的反应，导致短暂的缺血期，随后局部血管充血，结缔组织重塑，以巨噬细胞为代表的炎症细胞侵袭[9-11]。此外，持续的炎症会导致慢性组织损伤和重塑，从而导致癌症、关节炎、肥胖、糖尿病和神经变性等疾病[12-13]。因此，早期呼吸道炎症亟需高分辨率、深穿透性的成像方式，以提高急

性呼吸道炎症机理方面的理解，助力临床新型药物和创新治疗方案的研发。

在生物医学影像中，多种成像方法可以提供生物体内的各种微观和宏观现象，如核磁共振成像、X射线计算机断层成像、正电子发射断层成像、超声（US）成像、光学相干断层成像（OCT）、荧光成像（FI）等。这些成像技术在特异性、分辨率以及辐射等方面存在局限性，因此在疾病早期发展过程中，它们缺乏对生物结构的精细成像能力[14]。光声成像（PAI）是一种通过检测光声信号来实现激光照射组织的无创可视化技术。激光激发和超声检测的结合提供了前所未有的可扩展性[15-16]。实质上，PAI和US成像共用声学接收部分，不同之处在于US成像对比度反映组织的机械和弹性特性，而PAI反映组织的光学特性，特别是光学吸收。因此，PAI提供了比传统US成像更大的特异性，能够检测血红蛋白、脂质、水和其他吸光色素。然而，与纯光学成像方式（如OCT和FI）相比，PAI具有更大的穿透深度[17]。除了可视化微血管等解剖结构外，PAI还可以通过内源性[18]和外源性[19]造影剂等发色光团实现血氧、血流和温度等形式的功能成像。所有这些功能都可以在微米到厘米的宽尺度上实现，并具有可扩展的空间分辨率。这些属性使PAI在进行炎症成像时，在生理和病理的诊断、分期和监测方面比目前传统的

临床方法更具优势[20-25]。

吲哚菁绿（ICG）用于生物成像，是 PAI 研究中应用最广泛的一种外源性造影剂。作为唯一被美国食品药品监督管理局批准的菁染料，已广泛用于实体瘤、转移瘤的手术导航以及恶性组织的治疗[26-28]。ICG 的优异性能得益于其在近红外区域（NIR）的优异荧光特性和活性氧（ROS）或辐照下的高温效应。在本研究中，我们使用水解后的纳米态 ICG（Nano-ICG），该物质能够与炎症细胞结合起来，在临床试验中发挥作用。

巨噬细胞是免疫平衡行为的关键组成部分，它不仅通过识别病原体抑制呼吸道感染，而且能调节呼吸道内环境的稳定，还可以利用负反馈机制预防呼吸道炎症[29]。因此，巨噬细胞是免疫介导治疗的有效靶点，特别是当呼吸道屏障功能受损而引发异常炎症反应时[30]。本文利用巨噬细胞在炎症区域的高表达来表征呼吸道炎症的发展情况。

我们通过在气管内滴注 LPS 来模拟气道急性炎症损伤过程，通过 PAI 技术分析 LPS 滴注 2 d 后呼吸道炎症的变化。本文基于巨噬细胞可捕获外源性发光团 Nano-ICG 的功能特征，利用 Nano-ICG 增强 PAI 信号，如图 1 所示。通过建立动物模型并进行体内实验，定量评估了急性呼吸道感染中巨噬细胞的表达量，期望为急性呼吸道感染的炎症无创定量评估提供新的途径。
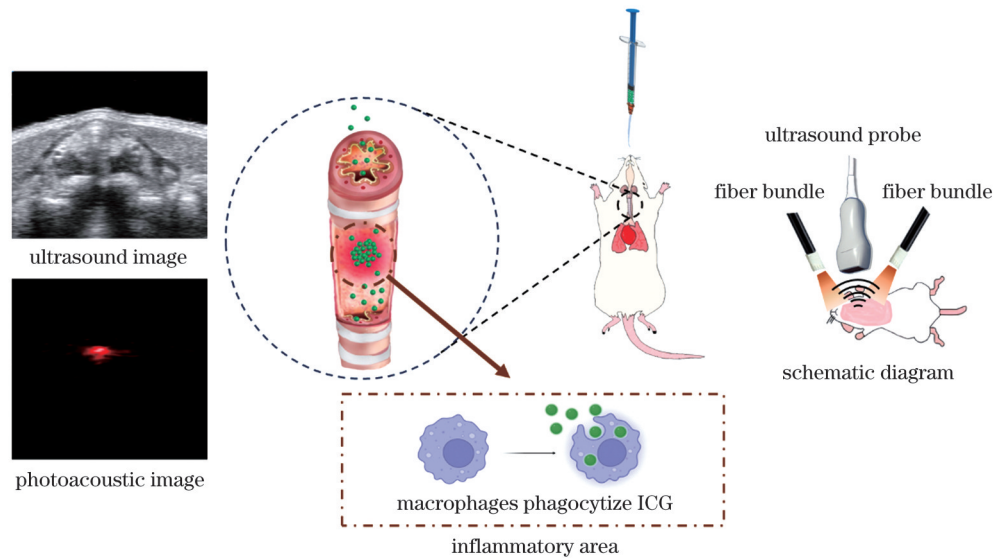

图 1 基于 Nano-ICG 的急性呼吸道感染光声成像的示意图
Fig. 1 Schematic of photoacoustic imaging of acute respiratory infection based on Nano-ICG

2 材料仪器

2.1 光声成像装置

本研究使用光声（PA）超声双模小动物成像系统对小鼠呼吸道进行 US-PA 双模成像。宽带换能器（频率范围为 18～38 MHz，中心频率为 30 MHz）用于 PAI，其空间分辨率可达 50 μm。该系统不仅具有高分辨率，还包含了"B-Mode""C-Mode""M-Mode""PA-Mode"等多种模式，可以对血氧饱和度、血流动力学及生理数据进行功能成像和监测。

2.2 研究对象

选取健康成年雄性昆明小鼠，鼠龄为 8～12 周，体重为 35～45 g，共 10 只。本研究的伦理许可证（编号为 GY2023-218）由广州医科大学机构动物护理和使用委员会提供。实验动物购入后，饲养于广州医科大学动物实验中心，饲养温度为 22～29 ℃，相对湿度为 40%～70%，新鲜空气每小时换气 10 次，采光时间为 12 h 白天和 12 h 黑夜的交替循环[31]。每个鼠笼内的垫料每天更换 1 次，实验鼠自由饮食，所有垫料和鼠维持配合饲料均由广东省医学实验动物中心提供。实验期间，保持饲养室内环境稳定，尽量避免实验受其他因素干扰。

2.3 试剂配制

脂多糖 LPS（来自大肠杆菌 055:B5 品系，质量浓度为 2 mg/mL）购于美国 Sigma 公司。ICG 购于上海源叶生物科技有限公司。H&E 染色液购于上海源叶生物科技有限公司。动物麻醉用异氟烷购于北京城林生物科技有限公司。细胞计数试剂盒购于北京全式金生物技术有限公司。

3 实验方法

3.1 动物模型的构建

经过 7 d 的适应性喂养后，将 10 只动物随机分成 2 组，每组 5 只，分为健康对照（Control）组和 LPS 造模（Model）组。Model 组通过鼻腔吸入给药。首先，先用体积分数为 1.5% 的异氟烷将小鼠麻醉；然后，将小鼠竖直悬挂于操作台上，将注射器的前端套上细导管，通过细导管向 Model 组小鼠的气管滴注 100 μL 的 LPS

溶液[32-33]。滴注后立即将小鼠上下往复颠倒,以确保药物均匀分布于呼吸道壁。小鼠基本清醒后,将其放回饲养笼。

3.2 细胞实验方案

采用细胞计数试剂盒测定 Nano-ICG 对巨噬细胞(RAW264.7 品系)的活性影响。巨噬细胞被接种在 96 孔板上(每个孔有 $2×10^4$ 个细胞,体积为 100 μL)。12 h 后将孔中的巨噬细胞放在不同质量浓度(0、110、220、330 μg/mL)的 Nano-ICG 水溶液中孵育 24 h。24 h 后加入细胞计数试剂(体积为 10 μL),每孔孵育巨噬细胞 3 h。用酶标记仪测定每个孔的吸光度,并测定巨噬细胞活力。

为了评价巨噬细胞对 Nano-ICG 的摄取能力,将小鼠单核巨噬细胞白血病细胞(RAW264.7 品系)接种于共聚焦皿上(共有 $5×10^4$ 个细胞),12 h 后用 Nano-ICG 溶液(体积为 50 μL,质量浓度为 2 mg/mL)进行孵育。通过激光共聚焦显微镜观察孵育前后的成像结果,判断巨噬细胞的吞噬情况。

3.3 呼吸道成像方案

采用 US-PA 双模小动物成像系统对 Control 组和 Model 组小鼠的呼吸道进行成像。PAI 信号通常由内源性吸收剂如黑色素、氧合血红蛋白和脱氧血红蛋白的光吸收主导[32-33],为了增加其他组织的信号,通常采用外源性造影剂,包括纳米粒子和染料[34-35]。Nano-ICG 作为一种外源性造影剂,能与细胞表面受体结合,从而在组织内实现均匀的积累,实现增强 PAI 成像。成像过程采用体积分数为 1.5% 的异氟烷麻醉小鼠,随后将颈部脱毛的小鼠置于成像平台上,在颈部正面涂抹超声耦合凝胶,进行成像实验。

LPS 滴注 2 d 后建模成功的 Model 组小鼠和健康状态的 Control 组小鼠各有 5 只,分别在滴注 Nano-ICG 前后进行 PAI 和 US 联合成像。每一组成像的采集时间点包括滴注后的 15、30、60 min。实验结束后,通过安乐死处死所有小鼠,以获取气道样品用于病理实验。利用 Vevo Lab Software 3.2.0 对实验采集的 PAI 和 US 成像数据进行离线定量分析。

在滴注 LPS 2 d 后的小鼠呼吸道内注入 100 μL 的质量浓度为 2 mg/mL 的 Nano-ICG,60 min 后取出气管,利用小动物活体荧光成像系统观察 Nano-ICG 富集在气管的情况(激发光波长为 745 nm,发射光波长为 840 nm),验证炎症细胞的发展程度。

3.4 病理实验

解剖出的小鼠气管首先被放置在标记好的包埋盒中,然后置于组织固定液中固定 24 h,随后在流水中冲洗 24 h。将经过流水冲洗处理的小鼠样品按照标准流程进行脱水处理,并包埋成蜡块。将包埋好的蜡块固定于旋转切片机上,并将其切成厚度为 4 μm 的薄片。染色前,将切片放入 60 ℃ 恒温箱中烤 2 h,再按 H&E 染色标准进行染色。最后,使用数字病理玻片扫描仪对染色后的切片进行图像采集并保存。对小鼠气管不同位置进行连续切片,尽可能多地获取整条气管的横断面和水平面染色图片,便于后期与光声成像结果进行对比。

3.5 数据测量和分析

本研究采用 Origin 软件对 PAI 强度数据进行统计分析。采用 Kruskal 统计法测定 4 个亚组(无 ICG 滴注、滴注后 15 min 组、滴注后 30 min 组和滴注后 60 min 组)的 PAI 强度的差异,数值以平均值±标准差(SD)表示。

4 实验结果

4.1 Nano-ICG 的表征

ICG 易溶于水,溶于水后形成纳米态 Nano-ICG,呈现绿色,首先通过透射电镜对外源造影剂 Nano-ICG 的形状及大小进行表征。如图 2(a)所示,Nano-ICG 的平均尺寸为 65 nm 左右,且呈现圆形,表现出聚集状分布。
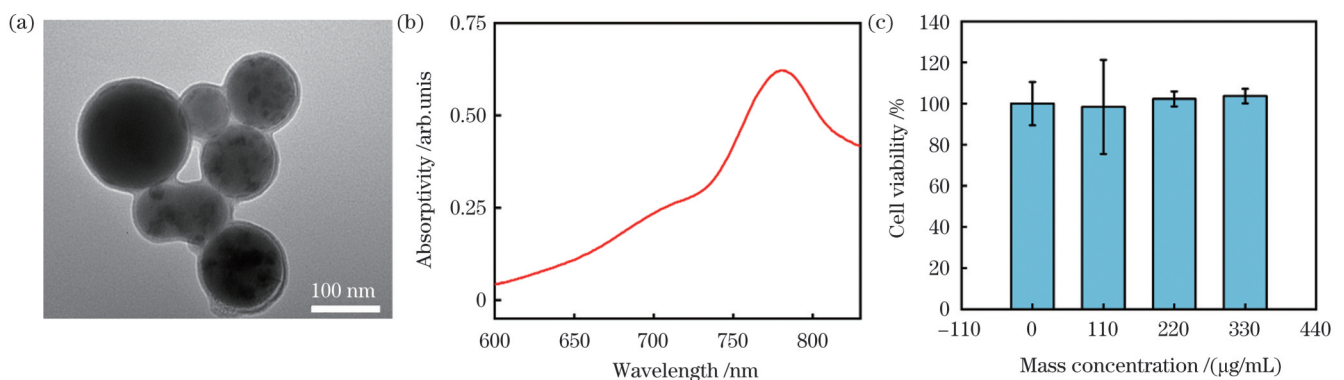

图 2 Nano-ICG 的表征。(a)Nano-ICG 颗粒的透射电镜(TEM)图;(b)Nano-ICG 在 600 和 850 nm 之间的紫外吸收光谱;(c)Nano-ICG 的细胞毒性测定

Fig. 2 Characterization of Nano-ICG. (a) Transmission electron microscopy (TEM) plots of Nano-ICG particles; (b) UV absorption spectra of Nano-ICG between 600 and 850 nm; (c) cytotoxicity testing of Nano-ICG

接下来，我们研究了 Nano-ICG 材料在不同波长照射下的紫外吸收光谱和细胞毒性。光学吸收性能是 PAI 对比度的主要决定因素。如图 2(b)所示，在 600～850 nm 区间，Nano-ICG 在 780 nm 处有最大的光吸收特性。随后对 Nano-ICG 的生物安全性进行了测试，实验结果如图 2(c)所示，质量浓度为 330 μg/mL 的 Nano-ICG 溶液对小鼠巨噬细胞没有毒性。

4.2　巨噬细胞对 Nano-ICG 的吞噬情况

我们通过实时成像进一步研究巨噬细胞在 Nano-ICG 注入后的内吞动态情况。如图 3 所示，我们使用共聚焦荧光显微镜观察了不同时间段内 Nano-ICG 注入后的内吞过程。结果显示，在 Nano-ICG 注入后的 1 h 内，巨噬细胞内吞 Nano-ICG 的现象很明显。此外，激光共聚焦图像显示巨噬细胞对 Nano-ICG 的摄取量与时间呈正相关，吞噬纳米颗粒后图像的信号强度也相应增大。
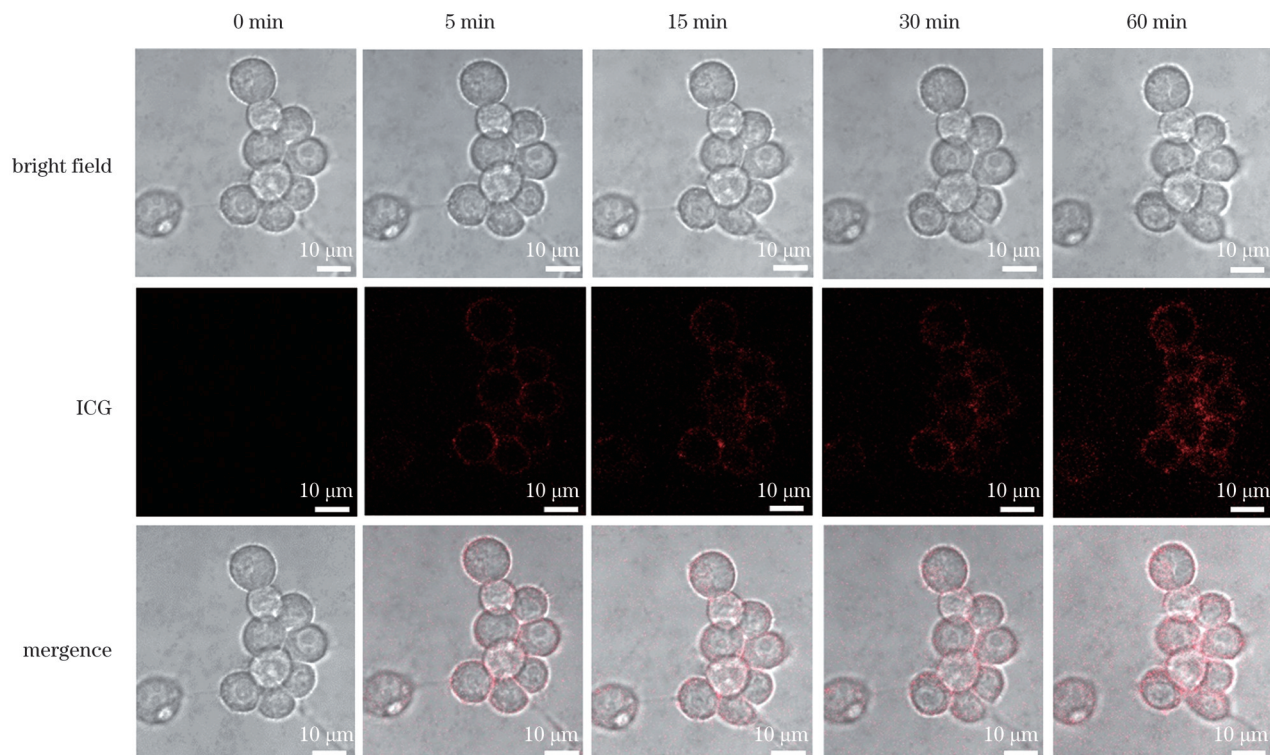

图 3　巨噬细胞在不同时刻处吞噬 Nano-ICG 的共聚焦成像结果

Fig. 3　Confocal imaging results of Nano-ICG phagoidities of macrophages at different moments

4.3　气道活体成像结果

本研究获取了 Control 组和 Model 组在 Nano-ICG 滴注前和滴注后 15、30、60 min 时的小鼠气道的 PAI 和 US 图像。如图 4(a)所示，小鼠在滴注 Nano-ICG 溶液 15 min 后，Model 组的 PAI 信号相较于 Control 组呈现增强的趋势。此外，在 Control 组中，随着时间的增加，Nano-ICG 的 PAI 信号呈现减弱的趋势。而在 Model 组中，对应 PAI 信号却不断增强。30 min 后，PAI 图像在 Control 组和 Model 组中呈现更明显的对比度。60 min 后，Model 组中的 PAI 信号最强，与 Control 组相比有更为显著的对比效果。

为了准确计算 Nano-ICG 增强呼吸道炎症的光声效果，本研究利用 PAI 图像测量不同时间下的信号强度。如图 4(b)所示，在 Control 组中，小鼠呼吸道内的 Nano-ICG 随着滴注后时间的增加不断地减少。如图 4(c)所示，在 Model 组中，小鼠呼吸道内的 Nano-ICG 随着滴注后时间的延长不断地增加。结果表明，Nano-ICG 在注入 60 min 后能有效地反映呼吸道壁上炎症细胞的发展程度。

本研究进一步利用 Matlab 软件对二维 PAI 图像进行了三维重建，如图 5(a)所示。三维呼吸道炎症的 PAI 结果可以提供更准确的呼吸道炎症信息。二维 PAI 扫描获得的冠状图显示，在呼吸道中此位置处有炎症细胞聚集，并显示了呼吸道中无炎症区域的 PAI 结果。图 5(b)展示了我们使用小动物荧光成像系统对滴注 Nano-ICG 后的小鼠炎症离体气道的成像结果。此成像结果为荧光成像数据叠加在白光成像上的伪彩图像，其中灰阶图像为使用该成像系统对上述小鼠气道进行白光成像的结果，伪彩色图像为使用该成像系统对上述小鼠气道进行荧光成像的结果。通过该结果，我们能够观察到气道中有炎症细胞处和无炎症细胞处的图像信息。
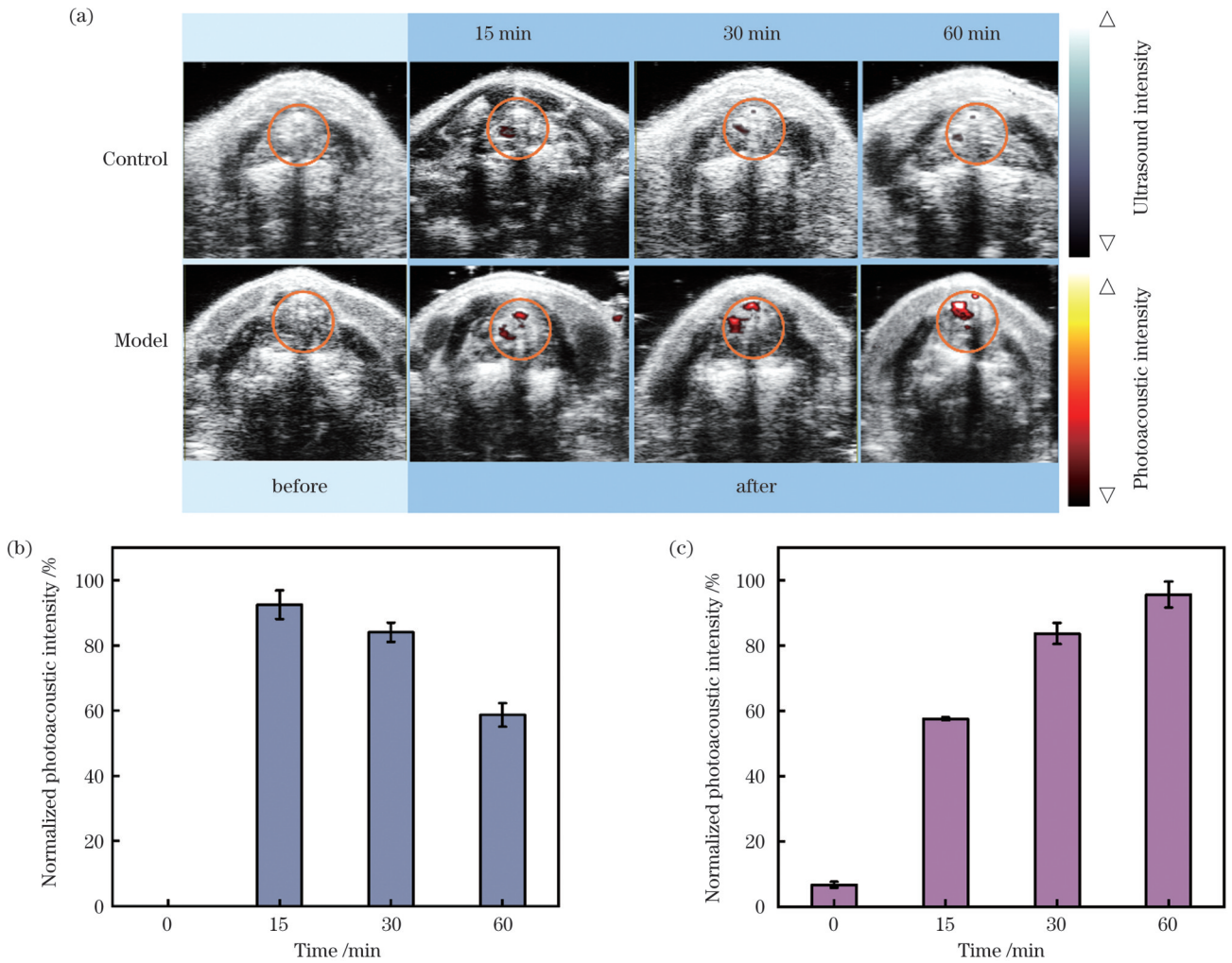
图 4　Control组和 Model组的 PAI结果以及分析结果。(a)Control组和 Model组在 Nano-ICG注入前和注入后的小鼠呼吸道的 PAI和 US图像的整合图像;(b)Control组中小鼠呼吸道内的 Nano-ICG数量随注入时间的变化;(c)Model组中小鼠呼吸道内的 Nano-ICG数量随注入时间的变化

Fig. 4　PAI and analysis results of Control group and Model group. (a) Integrated images of PAI and US images of mouse airways before and after Nano-ICG injection in Control and Model groups; (b) number of Nano-ICG in airway of mice in Control group versus injection time; (c) number of Nano-ICG in airway of mice in Model group versus injection time
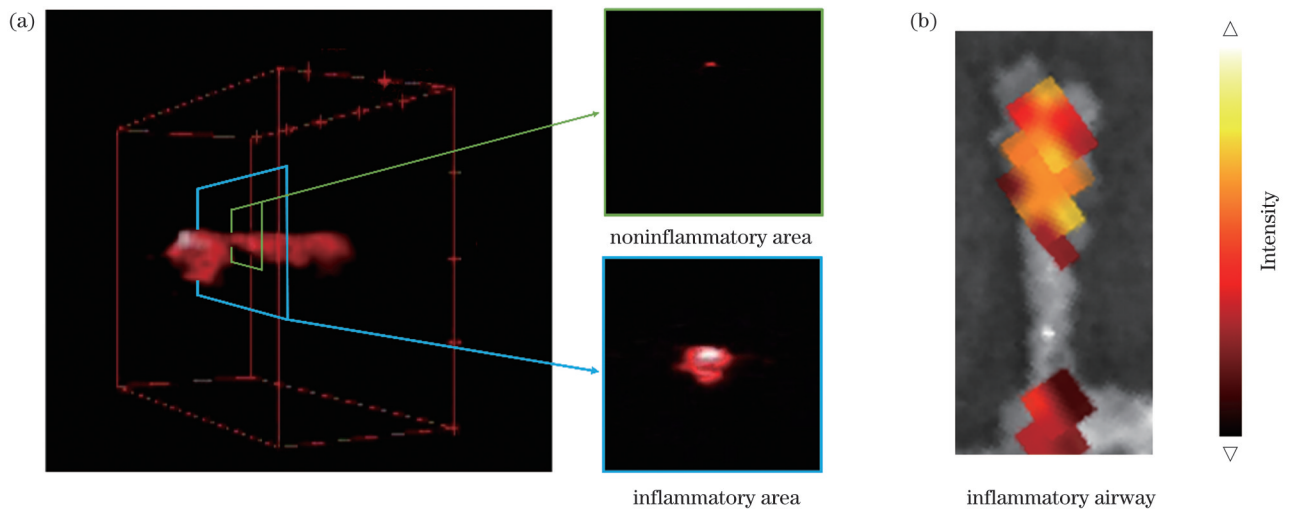

图 5　小鼠呼吸道的 PAI结果。(a)在 LPS滴注后第 2天小鼠呼吸道的三维 PAI图像;(b) Nano-ICG标记的炎症呼吸道的荧光图像

Fig. 5　PAI results of mouse airway. (a) Three denominational PAI images of mouse airway on second day after LPS instillation; (b) fluorescent image of inflamed airway labeled by Nano-ICG

4.4　呼吸道炎症的组织学评价

为了更进一步明确炎症引起的形态及结构的改变，本研究对气道样本进行病理切片和染色，结果如图 6 所示。在 Control 组的切片中，呼吸道呈浅粉色，管壁内侧无增厚，光滑平整，未观察到肿胀点和出血点，未见明显病变。相反，在 Model 组的切片中，呼吸道出现明显的出血和肿胀现象，表面散布出血点，管壁内侧炎症细胞浸润显著，管腔内分泌物增多，管壁及基底膜增厚不规则。
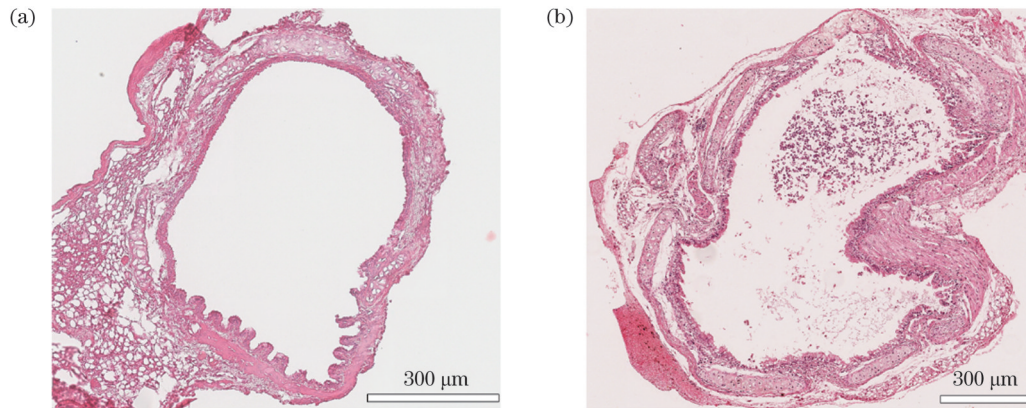

图 6　Control 组和 Model 组呼吸道切片染色结果的对比。(a)Control 组；(b)Model 组

Fig. 6　Comparison of staining results of respiratory tract sections between control group and model group. (a) Control group; (b) Model group

5　讨　　论

呼吸道感染是目前临床上常见的呼吸疾病之一。然而，对于这类疾病，我们仍缺乏有效的定量评估手段，这限制了临床治疗方法的应用。气管上皮不仅是呼吸道传递外界气体的枢纽，同时还参与气管的免疫反应，与管腔内的外液共同构成了第一道物理屏障，维持着呼吸系统的稳态[36]。病毒、细菌、灰尘颗粒等外部物质暴露在气管，活化免疫细胞，引发炎症反应，导致炎症细胞浸润，进而上皮细胞大量凋落缺失[37]。在治疗呼吸道感染时，临床医师通常会使用抗生素。因此，精确和快速的影像学分析不仅是确诊依据，也是选择合理治疗方案的基础，有助于减少过度使用抗生素。

研究表明，病理学和细胞生物学技术可以有效反映呼吸道炎症的发展程度。尽管小动物荧光成像系统可以定量显示呼吸道不同位置的炎症情况，如图 5(b)所示，但是其应用离不开侵入式的测量方法。常规病理学在大多数情况下也足以有效地呈现呼吸道的炎症情况，如图 6 所示。然而，这些方法通常具有侵入性测量和较高成本的特点，无法在在体情况下实现对呼吸道炎症的实时检测。在本研究中，通过光声系统对呼吸道炎症进行成像，可以实时、无创且定量地评估呼吸道的炎症发展程度。

基于实验结果可以发现 Nano-ICG 在被细胞吞噬后不仅不影响光学效果，而且随着时间的增加，其光学性能更加显著，此结果与相关文献[38-41]报道一致。由于纳米颗粒进入细胞有复杂的内吞途径[42-43]，因此通过借助 Nano-ICG 外源性造影剂的光谱特点，可以增强 PAI 图像对呼吸道炎症的显示效果。三维成像结果进一步突出了 PAI 成像优势，能够清晰地分辨呼吸道不同位置的炎症情况。尽管本研究成功实现了呼吸道炎症的定量评估，但仍存在一些不足之处。对于小鼠呼吸道炎症模型，尚未深入研究 Nano-ICG 滴注对其造成的影响，这可能会影响 Model 组和 Control 组在 PAI 图像中的整体光强。未来的研究将解决 Nano-ICG 滴注呼吸道的方式，以减少此过程对呼吸道炎症模型的影响。

6　结　　论

构建了小鼠的急性呼吸道炎症模型，借助 Nano-ICG 对呼吸道炎症进行观察，证实了 PAI 技术评估炎症的可行，Model 组炎症的光声成像结果、病理结果以及荧光成像结果匹配良好。综上所述，所构建的模型为 PAI 在呼吸道炎症评估过程中的应用提供了新的方法和思路，具有广阔的应用前景。

参 考 文 献

[1]　Walker C L F, Rudan I, Liu L, et al. Global burden of childhood pneumonia and diarrhoea[J]. The Lancet, 2013, 381(9875): 1405-1416.

[2]　World Health Organization. Facts sheet: pneumonia in children[R]. Geneva: WHO, 2022.

[3]　Ruuskanen O, Lahti E, Jennings L C, et al. Viral pneumonia[J]. Lancet, 2011, 377(9773): 1264-1275.

[4]　穆林, 向旭东. 细菌感染在慢性阻塞性肺疾病急性加重中的作用研究[J]. 长治医学院学报, 2008, 22(4): 308-311.
Mu L, Xiang X D. Study on the role of bacterial infection in acute exacerbation of chronic obstructive pulmonary disease[J]. Journal of Changzhi Medical College, 2008, 22(4): 308-311.

[5]　孙瑜, 卢建. 肺表面活性物质在支气管哮喘中的研究进展[J]. 临床肺科杂志, 2005, 10(3): 356-358.
Sun Y, Lu J. Research progress of pulmonary surfactant in bronchial asthma[J]. Journal of Clinical Pulmonary Medicine, 2005, 10(3): 356-358.

[6]　Long Y, Xiang Y, Liu S Y, et al. Baicalin liposome alleviates

lipopolysaccharide-induced acute lung injury in mice via inhibiting TLR4/JNK/ERK/NF-κB pathway[J]. Mediators of Inflammation, 2020, 2020: 8414062.

[7] Lei J J, Wei Y L, Song P C, et al. Cordycepin inhibits LPS-induced acute lung injury by inhibiting inflammation and oxidative stress[J]. European Journal of Pharmacology, 2018, 818: 110-114.

[8] Cheng K P, Yang A J, Hu X H, et al. Curcumin attenuates pulmonary inflammation in lipopolysaccharide induced acute lung injury in neonatal rat model by activating peroxisome proliferator-activated receptor γ (PPARγ) pathway[J]. Medical Science Monitor, 2018, 24: 1178-1184.

[9] Wilting J, Becker J, Buttler K, et al. Lymphatics and inflammation [J]. Current Medicinal Chemistry, 2009, 16(34): 4581-4592.

[10] Gupta S C, Kunnumakkara A B, Aggarwal S, et al. Inflammation, a double-edge sword for cancer and other age-related diseases[J]. Frontiers in Immunology, 2018, 9: 2160.

[11] Karin M, Clevers H. Reparative inflammation takes charge of tissue regeneration[J]. Nature, 2016, 529: 307-315.

[12] Hammoud D A. Molecular imaging of inflammation: current status [J]. Journal of Nuclear Medicine: Official Publication, Society of Nuclear Medicine, 2016, 57(8): 1161-1165.

[13] Willmann J K, van Bruggen N, Dinkelborg L M, et al. Molecular imaging in drug development[J]. Nature Reviews Drug Discovery, 2008, 7: 591-607.

[14] 穆根, 张振辉, 石玉娇. 生物医学影像中的光声成像技术[J]. 中国激光, 2022, 49(20): 2007208.
Mu G, Zhang Z H, Shi Y J. Photoacoustic imaging technology in biomedical imaging[J]. Chinese Journal of Lasers, 2022, 49(20): 2007208.

[15] Xu M H, Wang L V. Photoacoustic imaging in biomedicine[J]. Review of Scientific Instruments, 2006, 77(4): 041101.

[16] Huang G J, Lü J, He Y, et al. *In vivo* quantitative photoacoustic evaluation of the liver and kidney pathology in tyrosinemia[J]. Photoacoustics, 2022, 28: 100410.

[17] Jin X, Wang X K, Xiong K D, et al. High-resolution and extended-depth-of-field photoacoustic endomicroscopy by scanning-domain synthesis of optical beams[J]. Optics Express, 2019, 27 (14): 19369-19381.

[18] Jacques S L. Optical properties of biological tissues: a review[J]. Physics in Medicine and Biology, 2013, 58(11): R37-R61.

[19] Wu D, Huang L, Jiang M S, et al. Contrast agents for photoacoustic and thermoacoustic imaging: a review[J]. International Journal of Molecular Sciences, 2014, 15(12): 23616-23639.

[20] Liapis E, Klemm U, Karlas A, et al. Resolution of spatial and temporal heterogeneity in bevacizumab-treated breast tumors by eigenspectra multispectral optoacoustic tomography[J]. Cancer Research, 2020, 80(23): 5291-5304.

[21] Knieling F, Neufert C, Hartmann A, et al. Multispectral optoacoustic tomography for assessment of Crohn's disease activity [J]. The New England Journal of Medicine, 2017, 376(13): 1292-1294.

[22] Regensburger A P, Fonteyne L M, Jüngert J, et al. Detection of collagens by multispectral optoacoustic tomography as an imaging biomarker for Duchenne muscular dystrophy[J]. Nature Medicine, 2019, 25: 1905-1915.

[23] Fasoula N A, Karlas A, Kallmayer M, et al. Multicompartmental non-invasive sensing of postprandial lipemia in humans with multispectral optoacoustic tomography[J]. Molecular Metabolism, 2021, 47: 101184.

[24] Reber J, Willershäuser M, Karlas A, et al. Non-invasive measurement of brown fat metabolism based on optoacoustic imaging of hemoglobin gradients[J]. Cell Metabolism, 2018, 27 (3): 689-701.

[25] Fasoula N A, Karlas A, Prokopchuk O, et al. Non-invasive multispectral optoacoustic tomography resolves intrahepatic lipids in patients with hepatic steatosis[J]. Photoacoustics, 2023, 29:

[26] Wang H L, Li X X, Tse B W C, et al. Indocyanine green-incorporating nanoparticles for cancer theranostics[J]. Theranostics, 2018, 8(5): 1227-1242.

[27] Xue X D, Lindstrom A, Li Y P. Porphyrin-based nanomedicines for cancer treatment[J]. Bioconjugate Chemistry, 2019, 30(6): 1585-1603.

[28] Sheng Z H, Hu D H, Xue M M, et al. Indocyanine green nanoparticles for theranostic applications[J]. Nano-Micro Letters, 2013, 5(3): 145-150.

[29] Chelen C J, Fang Y, Freeman G J, et al. Human alveolar macrophages present antigen ineffectively due to defective expression of B7 costimulatory cell surface molecules[J]. The Journal of Clinical Investigation, 1995, 95(3): 1415-1421.

[30] Allard B, Panariti A, Martin J G. Alveolar macrophages in the resolution of inflammation, tissue repair, and tolerance to infection [J]. Frontiers in Immunology, 2018, 9: 1777.

[31] Lee C H, Cheng S H, Wang Y J, et al. Near-infrared mesoporous silica nanoparticles for optical imaging: characterization and *in vivo* biodistribution[J]. Advanced Functional Materials, 2009, 19(2): 215-222.

[32] Mracsko E, Stegemann-Koniszewski S, Na S Y, et al. A mouse model of post-stroke pneumonia induced by intra-tracheal inoculation with streptococcus pneumoniae[J]. Cerebrovascular Diseases, 2017, 43(3/4): 99-109.

[33] Beard P. Biomedical photoacoustic imaging[J]. Interface Focus, 2011, 1(4): 602-631.

[34] Zackrisson S, van de Ven S M W Y, Gambhir S S. Light in and sound out: emerging translational strategies for photoacoustic imaging[J]. Cancer Research, 2014, 74(4): 979-1004.

[35] Luke G P, Yeager D, Emelianov S Y. Biomedical applications of photoacoustic imaging with exogenous contrast agents[J]. Annals of Biomedical Engineering, 2012, 40(2): 422-437.

[36] Qamar W, Khan R, Khan A Q, et al. Alleviation of lung injury by glycyrrhizic acid in benzo(a)pyrene exposed rats: probable role of soluble epoxide hydrolase and thioredoxin reductase[J]. Toxicology, 2012, 291(1/2/3): 25-31.

[37] Ni Y F, Kuai J K, Lu Z F, et al. Glycyrrhizin treatment is associated with attenuation of lipopolysaccharide-induced acute lung injury by inhibiting cyclooxygenase-2 and inducible nitric oxide synthase expression[J]. Journal of Surgical Research, 2011, 165 (1): e29-e35.

[38] Ogawa M, Kosaka N, Choyke P L, et al. *In vivo* molecular imaging of cancer with a quenching near-infrared fluorescent probe using conjugates of monoclonal antibodies and indocyanine green [J]. Cancer Research, 2009, 69(4): 1268-1272.

[39] Nakajima T, Mitsunaga M, Bander N H, et al. Targeted, activatable, *in vivo* fluorescence imaging of prostate-specific membrane antigen (PSMA) positive tumors using the quenched humanized J591 antibody-indocyanine green (ICG) conjugate[J]. Bioconjugate Chemistry, 2011, 22(8): 1700-1705.

[40] Kobayashi H, Choyke P L. Target-cancer-cell-specific activatable fluorescence imaging probes: rational design and *in vivo* applications[J]. Accounts of Chemical Research, 2011, 44(2): 83-90.

[41] Harari D, Yarden Y. Molecular mechanisms underlying ErbB2/HER2 action in breast cancer[J]. Oncogene, 2000, 19(53): 6102-6114.

[42] Sahu R, Dixit S, Verma R, et al. A nanovaccine formulation of *Chlamydia* recombinant MOMP encapsulated in PLGA 85: 15 nanoparticles augments CD4$^+$ effector (CD44^{high} CD62L^{low}) and memory (CD44^{high} CD62L^{high}) T-cells in immunized mice[J]. Nanomedicine: Nanotechnology, Biology and Medicine, 2020, 29: 102257.

[43] Druzd D, Matveeva O, Ince L, et al. Lymphocyte circadian clocks control lymph node trafficking and adaptive immune responses[J]. Immunity, 2017, 46(1): 120-132.

100454.

Nondestructive Quantitative Assessment of Acute Airway Inflammation Based on Nano-ICG-Enhanced *In Vivo* Photoacoustic Imaging of Macrophages

Zhang Jian[1,2], Liang Chaohao[1], Luo Zhijia[1], Meng Fan[1], Zhang Yiqing[1], Wang Qian[1*]

[1]*Medical Imaging Innovation Laboratory, School of Biomedical Engineering, Guangzhou Medical University,*
Guangzhou 511436, *Guangdong, China;*

[2]*State Key Laboratory of Respiratory Diseases, First Affiliated Hospital, Guangzhou Medical University,*
Guangzhou 510120, *Guangdong, China*

Abstract

Objective Respiratory viruses possess strong infectivity, rapid transmission, short incubation periods, and sudden onset of illness. These features have led to widespread global transmission, significantly affecting the health of children worldwide. In addition, these viruses have caused significant economic losses and casualties in various countries. Antibiotics are commonly used to control respiratory infections in humans. Therefore, accurate and rapid understanding of the course of respiratory infections is the foundation for selecting a treatment plan.

In biomedical imaging, various imaging methods can reveal microscopic and macroscopic phenomena within organisms. These methods include magnetic resonance imaging (MRI), computed tomography, positron emission tomography, ultrasound (US) imaging, optical coherence tomography, and fluorescence imaging. These technologies provide rich information, thereby contributing to a comprehensive understanding of the characteristics of respiratory infections and supporting the development of rational treatment plans. Owing to limitations in specificity, resolution, and radiation, these imaging techniques lack the ability to accurately image biological structures in the early stages of disease development. In this study, the noninvasive, deep-penetrating, and high spatial resolution advantages of photoacoustic (PA) imaging (PAI) are utilized. This is combined with the excellent fluorescence properties of the exogenous contrast agent indocyanine green nanoparticles (nano-ICG) in the near-infrared region and the high expression of macrophages during inflammation. This combination enables the visualization of the development of respiratory inflammation.

Through the establishment of animal models and *in vivo* experiments, we quantitatively evaluate the macrophage expression in acute respiratory infections, as shown in Fig. 1. Research on PAI is expected to provide a new approach for the noninvasive quantitative assessment of inflammation in acute respiratory infections.

Methods This study uses a respiratory inflammation mouse model for photoacoustic imaging. Initially, the mice are anesthetized using isoflurane with volume fraction of 1.5%, followed by the instillation of lipopolysaccharide (LPS) solution into the mouse respiratory tract to construct the respiratory inflammation model group after two days. Five mice are selected from the Control and Model groups for further studies. Subsequently, the ultraviolet absorption spectra and cytotoxicity of nano-ICG materials are studied under irradiation at different wavelengths. The internalization dynamics of macrophages after nano-ICG injection are investigated. Finally, a PA-US dual-mode small animal imaging system is used to image different groups (Control and Model groups). Imaging is conducted before nano-ICG instillation and when the post-injection time is 15, 30, and 60 min in each group of mice. PA and US data collected from the experiment are subjected to offline quantitative analysis using Vevo Lab Software 3.2.0 to observe the overall respiratory inflammation under PAI.

Results and Discussions Transmission electron microscopy is used to characterize the shape and size of the exogenous contrast agent, nano-ICG. As shown in Fig. 2 (a), Nano-ICG has an average size of approximately 65 nm with a round shape and aggregated distribution. Subsequently, the cell counting kit is employed to evaluate the *in vitro* viability of macrophages, and the absorbance of each well is determined using enzyme-linked immunosorbent assay, as shown in Figs. 2(b) and 2(b). The internalization of nano-ICG at different time points after injection is observed using confocal fluorescence microscope, as shown in Fig. 3. These results indicate that nano-ICG continue to be internalized by the macrophages within one hour after injection. Additionally, laser confocal microscope images exhibit a positive correlation between the uptake of nano-ICG by macrophages and time. After engulfing the nanoparticles, the imaging effect of macrophages becomes more prominent. Within the first 15 min after nano-ICG injection in mice, Model group exhibits an enhanced trend in the PA signal compared with the normal group. In Control group, the PA signal of nano-ICG exhibits a decreasing trend over time, whereas in Model group, the corresponding PA signal continues to increase. After 30 min, the PAI images of Control and Model groups exhibit more noticeable contrast. After 60 min, Model group exhibits the strongest PA signal, showing a more significant contrast than Control group, as shown in Fig. 4(a). In Control group, the amount of nano-ICG in the mouse airways continuously decreases with increasing post-injection time, as shown in Fig. 4(b). In Model group, the quantity of nano-ICG on the mouse airway wall increases continuously with the post-injection time, as shown in Fig. 4(c). These results indicate that nano-ICG can effectively reflect the degree of development of inflammatory cells on the respiratory wall when the post-injection

time is 60 min. Three-dimensional PAI images of respiratory inflammation provide more accurate information on respiratory wall inflammation, as shown in Fig. 5(a). The coronal images generated by two-dimensional PAI scans, indicate the presence of inflammatory cell aggregation in the respiratory tract at that position. Figure 5(b) validates the accuracy of three-dimensional PAI images by showing images of inflammatory and non-inflammatory cells in the respiratory tract using an *in vivo* imaging system (IVIS) for small animals. Although PAI can visually present respiratory inflammation, some mice must be euthanized for pathological sectioning and staining to gain a more comprehensive understanding of the morphological and structural changes in inflammation. Histological results are shown in Fig. 6. Control group sections exhibit a light pink color in the airways with no thickening on the inner side of the tube wall and smooth and regular surfaces without apparent lesions. In contrast, Model group sections exhibit noticeable bleeding, significant swelling, scattered bleeding points on the surface, infiltration of inflammatory cells on the inner side of the tube wall, and increased secretion into the lumen, consistent with the imaging structures of PAI.

Conclusions　　This study successfully establishes a mouse model for acute respiratory inflammation and utilizes nano-ICG to observe respiratory inflammation, confirming the feasibility of evaluating inflammation using PAI. The PAI results for inflammation in the model are consistent with the pathological and IVIS results. This research provides new methods and insights for assessing respiratory inflammation. In summary, PAI is widely applicable to respiratory inflammation research because of its unique imaging capabilities, non-invasiveness, and high resolution. This study provides strong support for a deeper understanding of the development of respiratory inflammation and evaluation of treatment effectiveness.

Key words　　medical optics; photoacoustic imaging; acute airway inflammation; indocyanine green nanoparticles, macrophages